optica

Deep non-contact photoacoustic initial pressure imaging: supplementary material

PARSIN HAJI REZA[2,3], KEVAN BELL[1,3], WEI SHI[1], JAMES SHAPIRO[4] AND ROGER J. ZEMP[1,2]

[1]Department of Electrical and Computer Engineering, University of Alberta, Edmonton, Alberta, T6G 2V4, Canada
[2]Department of Systems Design Engineering, University of Waterloo, Waterloo, Ontario, N2L 3G1, Canada
[3]illumiSonics Inc., 1400-10303 Jasper Ave NW, Edmonton, AB, T5J 3N6, Canada
[4]Division of General Surgery, Faculty of Medicine and Dentistry, University of Alberta, 2000 College Plaza, 8215 -112 Street, Edmonton, AB T6G 2C8, Canada

Published 9 July 2018

This document provides supplementary information to "Deep non-contact photoacoustic initial pressure imaging," https://doi.org/10.1364/OPTICA.5.000814.

1. PARS Signal Magnitude Calculations

As an example, assuming a focal fluence of 500 mJ/cm^{-2} (used in previous work [1]), a red blood cell with 532 nm optical absorption (μ_a) of 587 cm^{-1} gives an initial pressure of 294 MPa (assuming unity Grüneissen parameter). For a planar-like red-blood-cell-plasma interface with this pressure rise an intensity reflection coefficient change of $\Delta R_I \approx 1.48 \times 10^{-3}$ is predicted, which at 1310-nm leads to a relative change in reflected light $\frac{\Delta R_I}{R_I} \approx 1.7$. This assumes $n_{\mathrm{RBC}} = 1.41$, $n_{\mathrm{Plasma}} = 1.33$, and $\delta n_{\mathrm{RBC}} = 0.055$ [2 – 5]. Relative to the reflectivity of an air-tissue interface (where tissue is considered as a air–water interface) $\frac{\Delta R_I}{R_I(\mathrm{Air-Tissue})} \approx 0.07$, which is closer to the measured modulation at the detector.

2. PARS Experimental Setup

Figure S1 shows PARS experimental setup. The output of a 1-ns pulse width, ytterbium-doped fiber laser (IPG Photonics) capable of pulse repetition rate from 20 to 600 kHz was coupled into a 4-m polarization-maintaining single-mode fiber (SMF) (HB-450, Fibercore Inc., UK) to generate stimulated Raman scattering (SRS) peaks using a fiber launch system (MBT621D/M, Thorlabs Inc.). SRS peaks are formed from inelastic nonlinear interaction between incoming photons through the fiber and the molecules in the fiber itself. A fiber optic spectrometer (USB4000, Ocean Optics Inc.) measured the SRS peaks and confirmed the spectrum. The output of the PM-SMF was collimated using a collimator lens (F280APC-A, Thorlabs Inc.).

A 1310-nm continuous diode laser with 40-µm-coherence length was used for detection. The beam was split by using a 90:10 in-line fiber splitter. The 10% of the light passes through an in-line variable attenuator and then connected to reference port of a balance photodiode. The 90% used to interrogate the reflected light from the sample with a spot which was co-focused with the excitation beam. The collimated interrogation beam passed through a polarized beam splitter (VBA05-1550, Thorlabs Inc., New Jersey) to direct vertically-polarized light through a $\lambda/4$ zero-order wave plate (Thorlabs Inc., New Jersey) into a beam combiner (BC) and was then scanned across the samples via a 2D galvanometer scanning mirror system (GVS012/M, Thorlabs Inc.) along with the excitation beam. The scanning mirrors were driven by a two-channel function generator (AFG3022B, Tektronix Inc.). The scanning light was then focused tightly using a 0.4-numerical-aperture objective lens (M Plan Apo NIR 20X, Mitutoyo, Japan). The light reflected back through the wave-plate converts from circular to horizontal polarization which then reflected at the polarizing beam-splitter interface directing maximum possible intensity of reflected light to a 75-MHz-bandwidth balanced photodiode (Thorlabs Inc., New Jersey)., 12-bit PCI digitizer (Gage Applied CSE1242) at a sampling rate of 200 MSamples/s. A two-axis mechanical scanning system was used for imaging larger fields-of-view. Two Micos PLS-85 linear stages each driven by an Anaheim Automation MBC25081 bipolar microstep driver provide lateral sample movement down to a 1.25 µm step size while maintaining scanning mirrors in a fixed position. Scanning region size was limited by the onboard capture card memory, though multiple captures or data streaming could be implemented to extend imaging range to the full reach of the motor stages.

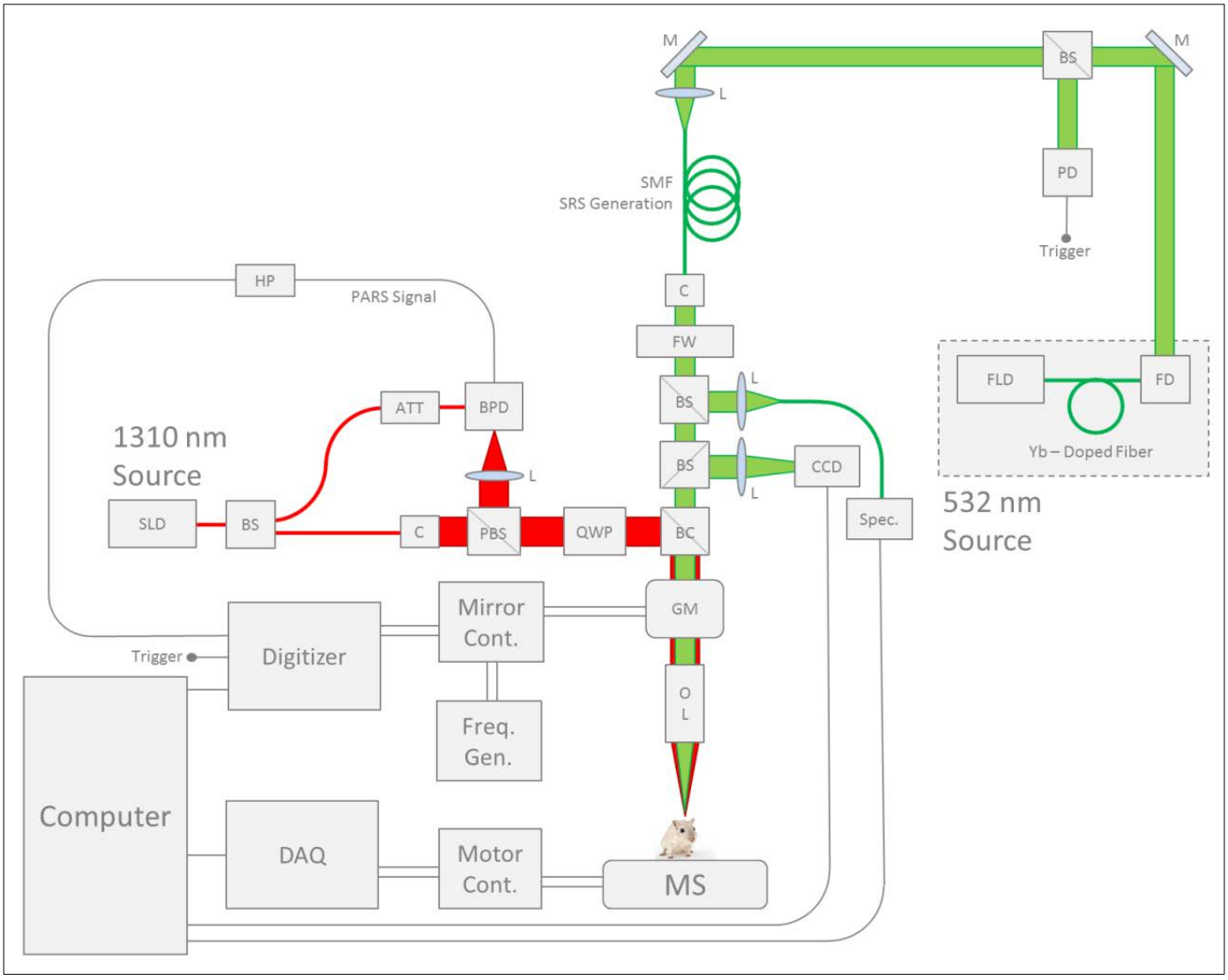

Figure S1: Functional PARS apparatus. | Excitation beam comes from a fiber laser driver (FLD) and is frequency doubled (FD) to provide 532 nm with ~1 ns pulses. The primary timing trigger is detected with a photodiode (PD). The beam is then focused into a polarization-maintaining single-mode fiber (SMF) where stimulated Raman scattering (SRS) takes place creating a spectrum at the fiber output which can consist of several peaks depending on input power and length of fiber used. A specific wavelength can be selected using a selection of band-pass filters mounted on a filter wheel (FW). The 1310 nm low-coherence probe beam is produced by a super-luminescent diode (SLD). Both beams are combined, then co-scanned using a galvanometer mirror (GM) system, and co-focused through an objective lens (OL). Scanning of larger regions can also be performed using a motor stage (MS). The PARS signal is collected at a balanced photodiode (BPD) then processed along with the mirror data and motor stage data to perform image reconstruction. A simple bright-field microscope is implemented using a CCD camera with matching focus to the interrogation location to view the sample and confirmation. Other elements include: Mirror (M), lens (L), linear polarizer (LP), bean splitter (BS), polarized beam splitter (PBS), attenuator (ATT), collimator (C), quarter wave plate (QWP), data acquisition card (DAQ).

3. Deep Imaging Approach

To investigate the imaging depth limit of PARS system, we compare the transport mean free path of 532 nm and 1310 nm, respectively. Transport mean free path l_t' is defined as [6]

$$l_t' = \frac{1}{\mu_t'} = \frac{1}{\mu_a + \mu_s'},$$

where μ_t' is transport interaction coefficient, μ_a is absorption coefficient, and μ_s' is reduced scattering coefficient. The wavelength dependence of μ_s' can be expressed as [7]

$$\mu_s'(\lambda) = a\left(\frac{\lambda}{500(\text{nm})}\right)^{-b}, \qquad (1)$$

where λ is wavelength in nm, and a and b are factors related to the scattering medium. Factor a is the value of μ_s' at λ = 500nm, which scales the wavelength-dependent term. Factor b is called scattering power.

For soft tissue ($a = 18.9\ \text{cm}^{-1}$, $b = 1.286$) [7], we have $\mu_s'(532\text{nm}) = 17.4508\ \text{cm}^{-1}$, $\mu_s'(1310\text{nm}) = 5.4768\ \text{cm}^{-1}$. Based on online published data, we use absorption coefficients in water to approximate the absorption coefficients in soft tissue [8]. Therefore, $\mu_a(532\ \text{nm}) = 0.000447\ \text{cm}^{-1}$,$\mu_a(1310\ \text{nm}) = 1.5348\ \text{cm}^{-1}$. Hence the transport mean free paths in soft tissue are calculated as $l_t'(532\ \text{nm}) = 0.57\ \text{mm}$, $l_t'(1310\ \text{nm}) = 1.43\ \text{mm}$.

For brain ($a = 24.2\ \text{cm}^{-1}$, $b = 1.611$) [7], we have $\mu_s'(532\ \text{nm}) = 21.8984\ \text{cm}^{-1}$, $\mu_s'(1310\ \text{nm}) = 5.1278\ \text{cm}^{-1}$.

Using the absorption coefficients in water to approximate the absorption coefficients in brain, the transport mean free paths in soft tissue are calculated as $l_t'(532\text{ nm}) = 0.46$ mm, $l_t'(1310\text{ nm}) = 1.50$ mm.

For the Intralipid solution (1%) used in our phantom studies, we use known information to estimate the corresponding factor a, b and then calculate the reduced scattering coefficient at 1310 nm. From online source [9], we average the reduced scattering coefficient between two curves for 10% Intralipid medium. Since $\mu_s'(500\text{ nm}) = 120\text{ cm}^{-1}, \mu_s'(700\text{ nm}) = 80\text{ cm}^{-1}$, we estimate $a = 120\text{ cm}^{-1}; b = 1.205$, and hence $\mu_s'(532\text{ nm}) = 111.3564\text{ cm}^{-1}$, $\mu_s'(1310\text{ nm}) = 37.5931\text{ cm}^{-1}$. For 1% Intralipid medium used in our phantom studies, $\mu_s'(532\text{ nm}) = 11.1356\text{ cm}^{-1}; \mu_s'(1310\text{ nm}) = 3.7593\text{ cm}^{-1}$. Hence the transport mean free paths in 1% Intralipis medium are calculated as $l_t'(532\text{ nm}) = 1.00$ mm, $l_t'(1310\text{ nm}) = 2.02$ mm.

4. Axial Resolution Characterization

To characterize the axial resolution of the PARS system, carbon fibers were embedded in gelatin at a depth of roughly 0.5mm. B-scanning was performed by scanning at progressive depths, forming a maximum amplitude signal projection at each scan depth. Figure S2 shows example B-scans of carbon fiber cross-sections used as point-spread functions. A vertical slice through a B-scan point-spread function was taken (as indicated by the white-dashed vertical line in S2). These data were fit to a Gaussian, and the 1/e width was calculated as 30 ± 5 μm.

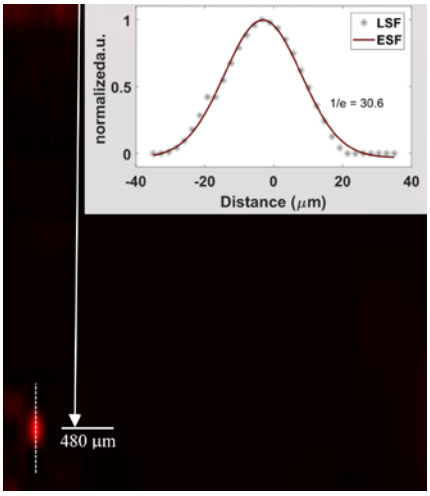

Figure S2: Axial resolution. | The depth of field (DOF) is experimentally measured as 30 ± 5 μm from scans of carbon fibers at a depth of 480 μm in gelatin.

References

[1] K. Maslov, F. H. Zhang, S. Hu, and L. Wang, "Optical-resolution photoacoustic microscopy for in vivo imaging of single capillaries," Opt. Lett. **33,** 929-931 (2008).

[2] G. S. Adair and M. E. Robinson, "The specific refraction increments of serum-albumin and serum-globulin," Biochemical Journal **24,** 993 (1930).

[3] J. Vörös, "The density and refractive index of adsorbing protein layers," Biophysical Journal **87,** 553–561 (2004).

[4] M. Friebel and M. Meinke, "Model function to calculate the refractive index of native hemoglobin in the wavelength range of 250-1100 nm dependent on concentration," Applied Optics **45,** 2838–2842 (2006).

[5] S. Prahl, "Optical Absorption of Hemoglobin" (1999), http://omlc.ogi.edu/spectra/hemoglobin/

[6] Wang LV, Wu H. Biomedical Optics: Principles and Imaging, Wiley, 2007.

[7] Jacques SL, "Optical properties of biological tissues: a review," Phys. Med. Biol. **58,** R37–R61 (2013).

[8] http://omlc.org/spectra/water/data

[9] http://omlc.org/spectra/intralipid/musp_intralipid.GIF